Yb_2Pt_2Pb: Magnetic frustration in the Shastry-Sutherland lattice

M. S. Kim,[1,2] M. C. Bennett,[2,3] and M. C. Aronson[1,2,3]
[1]*Condensed Matter Physics and Materials Science Department, Brookhaven National Laboratory, Upton, New York 11973-5000, USA*
[2]*Department of Physics, University of Michigan, Ann Arbor, Michigan 48109-1120, USA*
[3]*Department of Physics and Astronomy, Stony Brook University, Stony Brook, New York 11794-3800, USA*
(Received 16 July 2007; revised manuscript received 21 March 2008; published 23 April 2008)

We have synthesized single crystals of Yb_2Pt_2Pb, which crystallize in the layered U_2Pt_2Sn-type structure, where planes of Yb ions lie on a triangular network. Here, we report the results of magnetization, specific heat, and electrical resistivity experiments. The lattice constants and high temperature magnetic susceptibility indicate that the Yb ions are trivalent, while the Schottky peaks in the specific heat show that the ground state is a well isolated doublet. A significant magnetic anisotropy is observed, with the ratio of susceptibilities perpendicular and parallel to the magnetic planes differing by as much as a factor of 30 at the lowest temperatures. Antiferromagnetic order occurs at a Néel temperature $T_N=2.07$ K. Evidence of short range magnetic fluctuations is found in the magnetic susceptibility and electrical resistivity, which have broad peaks above T_N, and in the slow development of the magnetic entropy at T_N. Our experiments indicate that Yb_2Pt_2Pb is a quasi-two-dimensional and localized moment system, where strong magnetic frustration may arise from the geometry of the underlying Shastry-Sutherland lattice.

DOI: 10.1103/PhysRevB.77.144425 PACS number(s): 71.20.Eh, 75.30.Gw, 75.50.Ee

I. INTRODUCTION

Recently, a series of ternary compounds with composition R_2T_2M (R=rare earths or actinides; T=transition metals; M=Cd, In, Sn, and Pb) has attracted much attention because of the diversity of its collective phenomena, including ferromagnetic Kondo lattice,[1] Kondo semiconductor,[2] valence fluctuation,[3–6] non-Fermi liquid,[6,7] and heavy fermion ground states.[6,8,9] Most of this series crystallizes in the tetragonal Mo_2FeB_2-type structure (space group $P4/mbm$), which is an ordered derivative of the U_3Si_2 type. A smaller number of compounds crystallize in a distorted variant of this structure, the U_2Pt_2Sn-type structure (space group $P4_2/mnm$), which is a superstructure of the U_3Si_2 type.[10–15] Both structures are intrinsically layered, with two types of layers which are alternately stacked along the c axis. The first layer type contains only R atoms, while the second layer type contains only T and M atoms. In the first layer type, the R atoms are arranged in a triangular motif, giving each R atom a single nearest neighbor. This structure suggests that planes of magnetic dimers may be formed, which are necessary ingredients for novel spin liquid states, where frustration competes with order.

The crystal structure of the rare earth sublattices in both the Mo_2FeB_2 and U_2Pt_2Sn types suggests that they may be rare examples of the two-dimensional Shastry-Sutherland lattice, which has received substantial theoretical attention due to its exact dimerization and its spin liquid ground state.[16,17] Currently, there are only a few known materials known to be examples of the Shastry-Sutherland systems. One such system is $SrCu_2(BO_3)_2$, which has a layered structure where each Cu^{2+} ion is antiferromagnetically coupled to a single nearest neighbor and to four next nearest neighbors, with each unit cell containing two of these dimers, which are mutually orthogonal. Features of this dimerized lattice include the absence of magnetic order, the formation of a spin gap at low temperature, and the appearance of plateaux in the magnetization with 1/4, 1/8, and 1/10 of the full saturated moment,[18,19] as different ordered states emerge from the initially frustrated spin liquid through the application of magnetic fields.[17] Recently, similar plateaux have also been found in the magnetization of single crystalline TmB_4 and ErB_4, which form in the same space group as the layered Mo_2FeB_2-type structure, with the rare earth atoms forming the Shastry-Sutherland network.[20–23] Given this relationship between the Shastry-Sutherland lattice and the Mo_2FeB_2, U_2Pt_2Sn, and related crystal structure types, it is important to identify additional examples with different moment degeneracies and enhanced degrees of two dimensionality.

It is known that a number of different members of the R_2T_2M series with R=Ce, Yb, or U form in either the Mo_2FeB_2 or U_2Pt_2Sn structures. In order to ascertain their suitability as exemplars of the Shastry-Sutherland lattice, it is important to establish whether the fundamental attributes of magnetic anisotropy, dimerization, and geometrical frustration are present. So far, most studies on these latter compounds have been conducted on polycrystalline samples, precluding a definitive answer to this question. We have recently succeeded in synthesizing single crystals of Yb_2Pt_2Pb, which crystallize in the tetragonal U_2Pt_2Sn-type structure.[15] Here, we present a report of the anisotropic magnetization and magnetic susceptibility, the specific heat, and the electrical resistivity. We will argue here that the Yb moments in Yb_2Pt_2Pb lie on a lattice which is equivalent to the Shastry-Sutherland lattice.

II. EXPERIMENTAL DETAILS

Single crystals of Yb_2Pt_2Pb were grown from a Pb flux, forming in a rodlike morphology with a square cross section. Elements in the ration Yb:Pt:Pb=5:4:40 were placed in an alumina crucible and then sealed in an evacuated quartz tube. The materials were initially held at 1180 °C for 4 h and

TABLE I. Results of the crystal structure refinement for Yb_2Pt_2Pb.

Space group	$P4_2/mnm$ (No. 136)
Lattice parameters	$a=7.7651(6)$ Å
	$c=7.0207(7)$ Å
f.u./cell	$Z=4$
Cell volume	423.327 Å^3
Calculated density	14.80 g/cm^3
Conventional Rietveld reliability factors[a]	
$R_P=0.0976$, $R_{WP}=0.1290$, $R_{exp}=0.1145$	
$R_B=0.0361$, $R_F=0.0265$	
Goodness of fit	$\chi^2=1.28$

[a]R_P, profile factor; R_{WP}, weighted profile factor; R_{exp}, expected weighted profile factor; R_B, Bragg factor; and R_F, crystallographic factor.

subsequently cooled to 450 °C at 7 °C/h. Excess Pb was removed by centrifuging the tubes at 450 °C. Laue photoimages indicate that the crystallographic c axis ([001]) lies along the long axis of the crystal, while the a ([100]) and b ([010]) axes define the square cross section of the rod. An electron-probe microanalysis was carried out on polished single crystals by using a Cameca SX100 microprobe system with elemental Yb, Pt, and Pb standards. The atomic ratio of Yb:Pt:Pb is found to be $40.5\% \pm 0.3\%:39.2\% \pm 0.4\%:20.2\% \pm 0.5\%$ and is spatially uniform over the whole crystal surface. X-ray diffraction was performed on a powder prepared from the single crystals. The diffraction patterns were refined using FULLPROF. Refinement results and crystallographical data are listed in Tables I and II, respectively. Both confirm that Yb_2Pt_2Pb has the previously reported U_2Pt_2Sn-type structure.[15]

Magnetic susceptibility measurements were performed using a Quantum Design Magnetic Property Measurement System and a vibrating sample magnetometer (VSM) in a Quantum Design Physical Property Measurement System over temperature ranges $1.8\ \mathrm{K} < T < 300\ \mathrm{K}$ and $300\ \mathrm{K} < T < 800\ \mathrm{K}$, respectively. Magnetization measurements were performed using the VSM in magnetic fields of up to 14 T. The electrical resistivity was measured by the conventional four-probe method in the temperature range $0.4 < T < 300$ K. Specific heat measurements were carried out for temperatures between 0.4 and 100 K.

TABLE II. Crystallographic data for Yb_2Pt_2Pb at room temperature.

Atom	Wyckoff site	x	y	z	U_{eq}[a] (Å^2)
Yb1	4f	0.1771(8)	x	0	0.0074(23)
Yb2	4g	0.3386(8)	$-x$	0	0.0055(21)
Pt	8j	0.3730(3)	x	0.2747(9)	0.0066(9)
Pb	4d	0	1/2	1/4	0.0050(9)

[a]U_{eq} stands for the isotropic thermal parameter defined as one-third of the trace of the orthogonalized U_{ij} tensor.

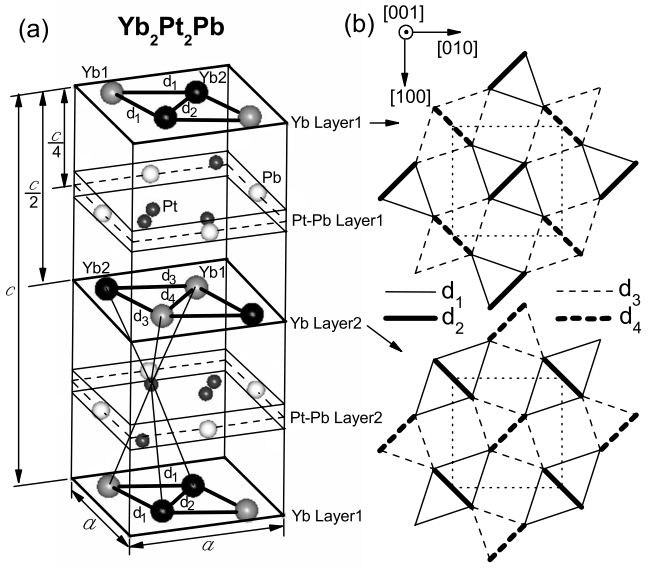

FIG. 1. (a) Schematic representation of the unit cell of Yb_2Pt_2Pb crystallizing in the tetragonal $P4_2/mnm$ (No. 136) structure. (b) Lattice structure of the Yb ions in Yb layers 1 (top) and 2 (bottom). The Yb ions lie at the vertices of the triangles and the dotted lines delineate the unit cell.

III. CRYSTAL STRUCTURE

In the tetragonal Mo_2FeB_2-type structure, T and M atoms of R_2T_2M lie in the same plane, while T atoms in the tetragonal U_2Pt_2Sn-type structure are displaced out of the plane, as demonstrated in the crystal structure of Yb_2Pt_2Pb shown in Fig. 1(a). Here, two of the four Pt atoms in the middle of the Pt-Pb plane are shifted down (up) and the other two close to the edge of the plane are shifted up (down) in Pt-Pb layer 1 (in Pt-Pb layer 2) without any shift of Pb atoms from the plane. These displacements result in two kinds of Yb-Pt tetrahedra, with large and small heights, as shown in Fig. 1(a). The shifted Pt atoms force the Yb atoms to form two different networks of isosceles triangles ($d_1=3.9646$ Å and $d_2=3.5451$ Å in Yb layer 1 and $d_3=4.1960$ Å and $d_4=3.8890$ Å in Yb layer 2), leading to a superstructural distortion with a doubled lattice parameter c. Among the rare earth and actinide intermetallics, only a few display a similar superstructural distortion.[10–15] On the other hand, in Yb layers 1 and 2, Yb atoms are arranged in the network of mixed rectangles and isosceles triangles, as shown in Fig. 1(b), implying that the two rare earth layers can separately be considered topologically similar to the Shastry-Sutherland lattices.[16] This suggests that magnetic frustration is likely to be an important feature of the magnetic behavior in Yb_2Pt_2Pb.

Figure 2 compares the structural parameters for some members of the R_2T_2M (R=rare earths, T=Pd and Pt, and M=Cd, In, and Pb) series,[4,5,15,24–26] which crystallize in the tetragonal Mo_2FeB_2-type structure, except for Yb_2Pt_2Pb which has the U_2Pt_2Sn-type structure. All parameters gradually decrease as the R atoms are changed from La to Lu due to the lanthanide contraction. For comparison, $c/2$,

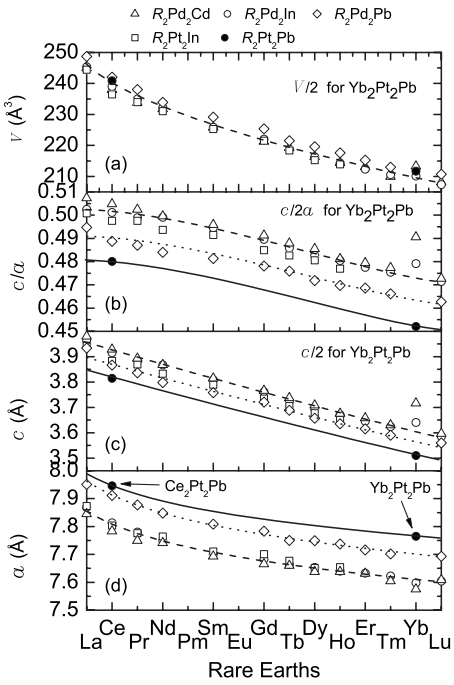

FIG. 2. Comparison of lattice parameters a and c, the ratio c/a, and the unit cell volume V for R_2T_2M (R=rare earths, T=Pd and Pt, and M=Cd, In, and Pb) (Refs. 4, 5, 15, and 24–26). Solid, dotted, and dashed lines are guides for the eyes.

$c/2a$, and $V/2$ are plotted for Yb_2Pt_2Pb. For lattice parameters a and c, we find the relation of $a(Pt,Pb)>a(Pd,Pb)>a(Pt,In)\gtrsim a(Pd,In)\gtrsim a(Pd,Cd)$ and $c(Pd,Cd)\gtrsim c(Pd,In)\gtrsim c(Pt,In)>c(Pd,Pb)>c(Pt,Pb)$. Considering atomic radii r ($r_{Pt}\gtrsim r_{Pd}$ and $r_{Pb}>r_{In}\gtrsim r_{Cd}$), this indicates that the increase in the sum of the radii of T and M atoms underlies the increase in the lattice parameter a and the decrease in the lattice parameter c. The inverse dependence of c compensates the dependence of a resulting in a much weaker variation in the unit cell volume with rare earth atom, as shown in Fig. 2(a). We note that the anomalously large values of c and c/a found in Yb_2Pd_2M (M=Cd and In) are caused by the intermediate valence of Yb in these compounds.[4–7] In contrast, the values of c and c/a in Yb_2Pt_2Pb are consistent with those of other compounds with trivalent rare earth ions. This indicates that Yb in Yb_2Pt_2Pb is in a stable trivalent Yb state, without a mixed valence character. From the unusually low value of c/a found in Yb_2Pt_2Pb, we anticipate a strongly anisotropic behavior.

Among the R_2Pt_2Pb (R=rare earth) series, only Ce_2Pt_2Pb (Ref. 26) and Yb_2Pt_2Pb have previously been reported. Note that Ce_2Pt_2Pb crystallizes in the tetragonal Mo_2FeB_2-type structure, while Yb_2Pt_2Pb forms in the distorted U_2Pt_2Sn-type variant. One might thus expect that R_2Pt_2Pb compounds composed of light rare earths R may crystallize in the tetragonal Mo_2FeB_2-type structure, while the heavy rare earths crystallize in the tetragonal U_2Pt_2Sn-type structure. A similar effect was observed in the R_2Au_2In series,[14] where only the heavy rare earths R=Tm and Lu crystallize in the tetragonal U_2Pt_2Sn-type structure. Considering the lanthanide contraction, this indicates that the small size of the heavy rare earth atoms plays an important role in enabling the superstructural distortion. Specifically, we suggest that the displacement of the T atoms in R_2T_2M with the tetragonal U_2Pt_2Sn-type structure only occurs for small R atoms. This proposal is supported by the observations that the compounds with divalent Yb (Yb_2Cu_2In and Yb_2Au_2In)[27,28] and the compounds with mixed valent Yb (Yb_2Pd_2Cd, Yb_2Pd_2In, and Yb_2Pd_2Sn),[4–7] where the Yb atoms all have relatively large size, instead crystallize in the Mo_2FeB_2-type structure and not in the U_2Pt_2Sn-type structure. Conversely, it seems that Yb atoms in the tetragonal Mo_2FeB_2-type structure prefer divalent or mixed valent states to the trivalent state, while Yb atoms in the tetragonal U_2Pt_2Sn-type structure prefer trivalent states. We note that Yb_2Pt_2Pb is the only one of the reported Yb compounds of R_2T_2M series which is trivalent. Recently, composition dependent magnetic order has been found in compounds of the series $Yb_2Pd_2In_{1-x}Sn_x$ for x=0.6 and 0.8, intermediate between the mixed valent endpoints Yb_2Pd_2In and Yb_2Pd_2Sn.[7] Also, applying pressures between 1 and 4 GPa causes Yb_2Pd_2Sn to order magnetically.[29] These observations of magnetic order imply that the Yb ions are trivalent. It would follow then that the crystal structures of these compounds may well be distorted from the tetragonal Mo_2FeB_2-type structure, possibly into the U_2Pt_2Sn-type structure found in Yb_2Pt_2Pb. It would be interesting to test for such a structural change in these magnetically ordered compounds.

IV. PHYSICAL PROPERTIES

A. Experimental results

Figure 3(a) shows the inverse of the magnetic susceptibilities $1/\chi_{[100]}$ and $1/\chi_{[001]}$, which are measured with a magnetic field B=0.1 T along [100] and [001], respectively, below 800 K. The data between 300 and 800 K are well described by a modified Curie–Weiss law $[\chi=\chi_0+C/(T-\theta)]$, which gives $\chi_0=-0.0006$ emu/Yb mol, a Weiss temperature $\theta_{[100]}=28$ K, and an effective moment $\mu_{eff}=4.42\mu_B$ for $1/\chi_{[100]}$, while $\chi_0=-0.0004$ emu/Yb mol, $\theta_{[001]}=-217$ K, and $\mu_{eff}=4.54\mu_B$ for $1/\chi_{[001]}$. The effective moments deduced from $1/\chi_{[100]}$ and $1/\chi_{[001]}$ are very close to $4.54\mu_B$, as expected for free Yb^{3+} ions. This indicates that the Yb moments in Yb_2Pt_2Pb are well localized and trivalent at high temperatures, which are consistent with the analysis of the crystal structure.

Figure 3(a) shows that both $1/\chi_{[100]}$ and $1/\chi_{[001]}$ increasingly deviate from the Curie–Weiss behavior below 300 K and that this deviation is particularly marked for $1/\chi_{[001]}$. As indicated in Fig. 3(b), $\chi_{[001]}$ is nearly independent of temperature down to 30 K, with a magnitude of only $\sim 5\times 10^{-3}$ emu/Yb mol, displaying a residual tail at the lowest temperatures. For $1/\chi_{[100]}$, the deviation from the Curie–Weiss law is less pronounced and is only detected below 150 K. The inset of Fig. 3(b) shows $\chi_{[100]}$ and $\chi_{[001]}$ below 5 K. A broad maximum is found for $\chi_{[001]}$ and especially $\chi_{[100]}$ between 2 and 3 K, while a sharp cusplike anomaly is found in $\chi_{[001]}$ and a weaker anomaly in $\chi_{[100]}$, indicating the onset of magnetic order at 2.07 K.

The magnetic susceptibility is strongly anisotropic, with $\chi_{[100]}/\chi_{[001]}\sim 30$ at low temperatures, a value which is even

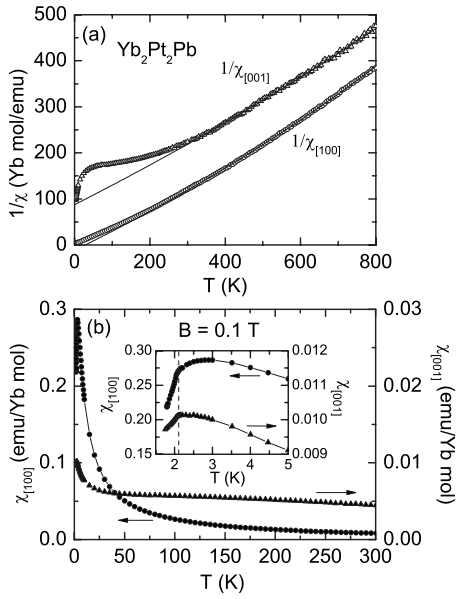

FIG. 3. (a) Temperature dependences of the inverse susceptibilities $1/\chi_{[100]}$ (○) and $1/\chi_{[001]}$ (△) up to 800 K. The magnetic susceptibility at 300 K$<T<$800 K was measured in 2 T. The solid lines represent a fit with a modified Curie–Weiss law at 300 K$<T<$800 K (see text). (b) Temperature dependence of magnetic susceptibilities $\chi_{[100]}$ (●) and $\chi_{[001]}$ (▲) for $B\|[100]$ and $B\|[001]$, respectively, below 300 K in 0.1 T. The inset shows an enlarged plot of $\chi_{[100]}$ and $\chi_{[001]}$ with $T<5$ K.

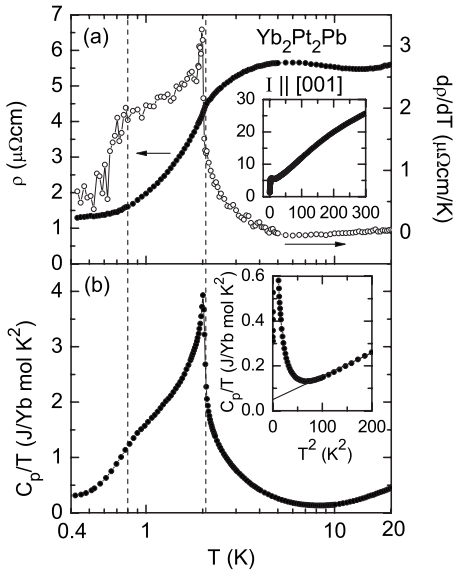

FIG. 5. (a) Logarithmic temperature dependence of the resistivity ρ (●) and the temperature derivative of the resistivity $d\rho/dT$ (○) below 20 K. The inset shows the temperature dependence of ρ over an expanded temperature range. (b) Logarithmic temperature dependence of the specific heat divided by temperature C_p/T below 20 K. The inset shows the plot of C_p/T vs T at high temperatures. Solid line in the inset indicates the fit of $C_p/T=\gamma_h+\beta T^2$ above 8 K.

larger than that found in R_2Cu_2In (R=Gd-Tm).[30] Figure 4(a) shows the field dependence of the magnetizations $M_{[110]}$, $M_{[100]}$, and $M_{[001]}$, which is measured at 1.9 K with the magnetic field oriented along the different principal directions, [110], [100], and [001]. It is clear that the magnetic hard axis is along [001], since here $M_{[001]}$ reaches only $0.25\mu_B$/Yb in fields as large as 14 T. In contrast, $M_{[110]}$ and $M_{[100]}$ gradually increase and then saturate at $2.6\mu_B$ and $1.9\mu_B$ above 5 and 3 T, respectively. This last observation indicates that [110] is the easy direction in the plane, while the limited anisotropy between the [110] and [100] directions shows that this anisotropy is very small compared to the anisotropy that confines the moments to the layers themselves.

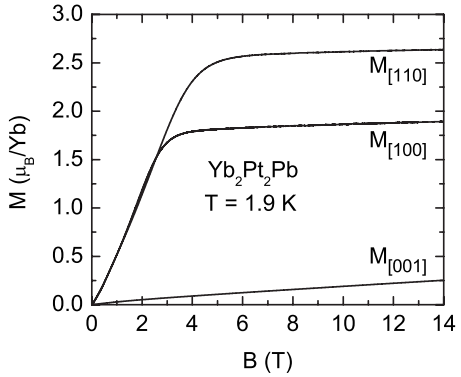

FIG. 4. (a) Magnetic field dependences of the magnetizations $M_{[001]}$, $M_{[100]}$, and $M_{[110]}$ for $B\|[001]$, $B\|[100]$, and $B\|[110]$, respectively.

The inset of Fig. 5(a) shows the temperature dependence of the electrical resistivity ρ with the current flowing along [001]. The resistivity is definitively metallic, gradually decreasing with a weak positive curvature from its initial value of 26 $\mu\Omega$ cm at 300 K. The resistivity of most polycrystalline compounds from the R_2T_2M series is very high, typically several hundreds of $\mu\Omega$ cm at 300 K and several tens of $\mu\Omega$ cm even at the lowest temperatures. For Yb_2Pt_2Pb, the much lower resistivity at 300 K indicates very good crystal quality and a near optimal growth of our single crystals. Figure 5(a) shows that with decreasing temperature, a shallow minimum is found in ρ at 13 K, followed by a broad maximum preceding the sudden drop at 2.07 K, the same temperature at which magnetic order is detected in $\chi_{[100]}$ and $\chi_{[001]}$. Additional evidence of magnetic order is found in the specific heat divided by temperature, C_p/T, where a sharp peak is found at 2 K, as shown in Fig. 5(b). Remarkably, Fig. 5(b) demonstrates that the temperature dependences of C_p/T and $d\rho/dT$ are virtually identical, both above and below the 2.07 K ordering temperature. Both show distinct shoulderlike anomalies near 0.8 K, terminating at the lowest temperatures in a residual resistivity $\rho_0=1.3$ $\mu\Omega$ cm and an electronic part of the specific heat $\gamma=311$ mJ/Yb mol K^2, respectively. Given the high quality of our crystals, we believe that the shoulderlike feature is intrinsic to Yb_2Pt_2Pb and does not result from the inclusion of a secondary phase. However, it proves impossible to fit these data over a convincing range of temperatures using any of the conventional expressions for spin waves, either with or without gaps.

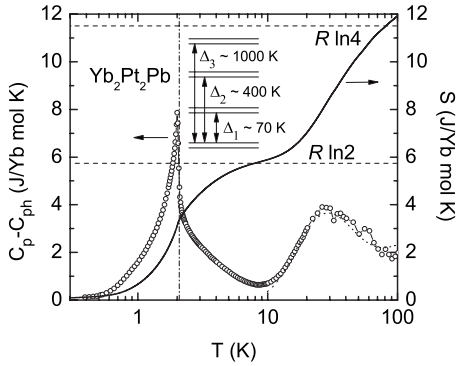

FIG. 6. The temperature dependence of the measured specific heat C_p from which we have subtracted an estimated phonon contribution C_{ph} and the associated entropy S. The dotted line represents a fit to a Schottky expression. The schematic diagram of the CEF levels from the fitting is presented in the inset.

Figure 6 shows the magnetic contribution of the specific heat $C_p - C_{ph}$, where C_{ph} is the phonon contribution of the specific heat estimated from the Debye model. The Debye temperature, $\theta_D = 184$ K, is obtained by fitting $C_p/T = \gamma_h + \beta T^2$ above 8 K, as shown in the inset of Fig. 5(b). The entropy S is only $0.58R$ ln 2 at 2.07 K. With increasing temperature, $C_p - C_{ph}$ shows a long tail up to 8 K at which a minimum is found and where the entropy S recovers its full value of R ln 2. The long tail between 2.07 and 8 K is consistent with the broad maxima in $\chi_{[100]}$ and ρ along [001] in indicating the presence of short range magnetic fluctuations in this temperature range. The entropy S remains approximately constant between 10 and 15 K, indicating that magnetic order develops from a well-separated doublet ground state. A broad maximum is found near 30 K in $C_p - C_{ph}$, which can be identified as a Schottky anomaly with an energy splitting scheme of $\Delta_1 \sim 70$ K, $\Delta_2 \sim 400$ K, and $\Delta_3 \sim 1000$ K between the four doublets expected for the crystalline electric field induced by the local $m2m$ symmetry of Yb sites in Yb_2Pt_2Pb, as shown in the inset of Fig. 6. With increasing temperature, S gradually increases and eventually reaches R ln 4 around 70 K, as expected, given the observation of the Schottky anomaly at 30 K. This scale of crystal field splitting is comparable to that found in inelastic neutron scattering measurements on Yb_2Pd_2In.[7]

B. Discussion

Our analysis of crystal structure trends in isostructural rare earth compounds provides indirect evidence that the Yb moments in Yb_2Pt_2Pb are trivalent. Magnetic susceptibility measurements confirm this result, finding a conventional paramagnetic state above ~300 K which involves fluctuations of the full Yb^{3+} moment. Specific heat measurements confirmed that the crystal electric field scheme is consistent with the local site symmetry for the Yb^{3+} moments. Further, these measurements indicate that the ground state of Yb_2Pt_2Pb involves a well isolated doublet for the Yb moments.

Cusplike anomalies in the magnetic susceptibilities $\chi_{[100]}$ and especially $\chi_{[001]}$ indicate the onset of antiferromagnetic order at 2.07 K. The Weiss temperature $\theta_{[001]}(=-217$ K), found when the field is perpendicular to the layers, is approximately an order of magnitude larger than the in-layer Weiss temperature $\theta_{[100]}(=28$ K). We conclude then that the anisotropy conferred on the Yb moments by the crystal electric field must be the dominant factor in establishing magnetic anisotropy in Yb_2Pt_2Pb, since the layered crystal structure would otherwise argue for weak interactions between planes and strong interactions in the moment-bearing planes, contradicting our observations that $\theta_{[001]}$ is an order of magnitude larger than $\theta_{[100]}$. Since it is not possible to deduce the strength of the intermoment interactions that ultimately drive the magnetic order from the magnetic susceptibility without a suitable theory, we only note that on temperature scales pertinent to the establishment of magnetic order, the interplay of strong single ion anisotropy with anisotropy in the intermoment interactions associated with the layered crystal structure is responsible for both the complex magnetic structure and its accompanying fluctuations. The temperature dependences of the specific heat and the temperature derivative of the electrical resistivity are nearly identical both above and below the magnetic transition. This implies that the resistivity is dominated by forward scattering, as expected in a system with an abundance of small-wave-vector critical fluctuations, such as a ferromagnet.[31] We conclude that the magnetic structure of Yb_2Pt_2Pb may be rather complex, with mixed antiferromagnetic and ferromagnetic characters, perhaps reflecting the geometrically frustrated nature of the Shastry-Sutherland lattice. One possibility for the zero-field structure would be a long-wave ferromagnetic spiral, as has been theoretically proposed.[32,33]

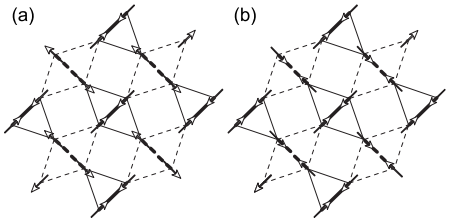

FIG. 7. Schematic representation of possible magnetic structures of the Yb layers: (a) U_2Pt_2Sn type and (b) GdB_4 type.

However, the underlying symmetries of the crystal lattice constrain the magnetic structure of Yb_2Pt_2Pb. Yb atoms occupy two inequivalent sites with local $m2m$ symmetry, lying at the intersections of the (001), (110), and $(1\bar{1}0)$ mirror planes. It is well known that magnetic moments must lie in mirror planes or be perpendicular to them. The very low values of $\chi_{[001]}$ and $M_{[001]}$ indicate that the magnetic moments of the Yb^{3+} ions in Yb layers lie in the (001) plane. By analogy to the magnetic structures of U_2Pt_2Sn and GdB_4,[34,35] the Yb moments are probably aligned along [110] and $[1\bar{1}0]$, in agreement with the anisotropy between the saturation moments of $M_{[110]}$ and $M_{[100]}$. Two possible magnetic structures which are consistent with these constraints are shown in Fig. 7.

The onset of antiferromagnetic order from a strongly frustrated paramagnetic state, as we observed in Yb_2Pt_2Pb, is consistent with theoretical expectations for the Shastry-

Sutherland model. The strong magnetic anisotropy confirms that the moments lie in the rare earth layers. In both layers, the Yb moments lie on a lattice of isosceles triangles with slightly different Yb spacings ($d_2 < d_1$ and $d_4 < d_3$). This separation of nearest Yb neighbors and next nearest Yb neighbors results in a separation of the antiferromagnetic exchange interactions ($J_1 < J_2$ and $J_3 < J_4$), leading to the formation of well-defined pairs of Yb nearest neighbors in the two rare earth layers [see Fig. 1(b)]. In this way, the arrangement of the rare earth ions in both layers in Yb_2Pt_2Pb is separately equivalent topologically to the lattice of the Shastry-Sutherland model. Accordingly, the magnetic structure inferred from the magnetization measurements (Fig. 7) consists of sheets of orthogonal Yb dimers.

There is considerable evidence of the influence of frustration on the magnetic properties of Yb_2Pt_2Pb. A universal feature of magnetically frustrated systems is that magnetic order occurs at temperatures that are much smaller than the scale of the interactions revealed by the Weiss temperatures. By this measure, Yb_2Pt_2Pb is highly frustrated, since the Weiss scale implies that the mean field interactions are more than 2 orders of magnitude stronger than the 2.07 K ordering transition. The broad maximum in $\chi_{[100]}$ just above the magnetic ordering temperature is also suggestive of the short range magnetic disorder common to systems with strong magnetic frustration. We have considered the possibility that the Kondo effect is responsible for these departures from ideal local moment behavior. Since it is a single ion phenomenon, manifestations of the Kondo effect should display no significant anisotropy. However, we see that the susceptibility maximum is most pronounced in $\chi_{[100]}$, suggesting that its origin must instead be related to the intrinsic magnetic anisotropy of Yb_2Pt_2Pb. In agreement with our results, similar maxima are found in the anisotropic susceptibilities of $SrCu_2(BO_3)_2$, TmB_4, and ErB_4 where the magnetic ions also lie on the Shastry-Sutherland network and where no Kondo effect is likely.[21,36] We conclude that the broad maximum in $\chi_{[100]}$ reflects the excess magnetic fluctuations in the moment-bearing planes, originating with the geometrically frustrated Shastry-Sutherland lattice. These fluctuations are also responsible for the slow recovery of the magnetic entropy above the ordering temperature, which are detected as long tails in the specific heat and electrical resistivity which extend to temperatures as large as ~10 K, i.e., five times the transition temperature itself.

The scenario in which long range antiferromagnetic order emerges from a frustrated magnetic liquid in Yb_2Pt_2Pb is consistent with our expectations of the Shastry-Sutherland lattice. Zero temperature calculations for spin-$1/2$ moments in the two-dimensional Shastry-Sutherland lattice[37] predict a quantum critical point when the ratio of the nearest neighbor J' and next nearest neighbor J exchange interactions $(J/J')_{QCP}=0.7$. As shown in Fig. 8, the quantum critical point separates a magnetically frustrated spin liquid for $J/J' < (J/J')_{QCP}$ from a Néel ordered ground state with $J/J' > (J/J')_{QCP}$. While there is little theoretical guidance regarding the finite temperature properties of the Shastry-Sutherland lattice, further increases of (J/J') beyond

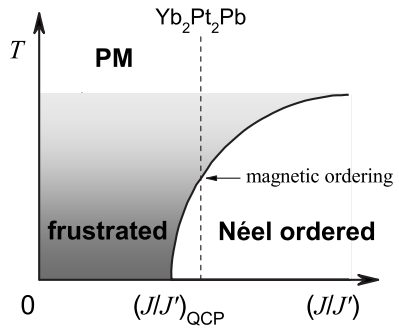

FIG. 8. Schematic phase diagram for the Shastry-Sutherland lattice (see text).

$(J/J')_{QCP}=0.7$ are presumed to stabilize the Néel ordered state at progressively higher temperatures, leading to the phase line qualitatively depicted in Fig. 8. If the dominant physics is that of the Shastry-Sutherland lattice, we assume that Yb_2Pt_2Pb lies in this limit, where antiferromagnetic order emerges from the spin liquid state. In order to establish this conclusively, we must experimentally rule out other factors such as structural modification, more distant neighbor exchange interactions, and the interlayer exchange itself as possible drivers of magnetic order in Yb_2Pt_2Pb.

V. CONCLUSION

We have presented the magnetic, transport, and thermal properties of single crystals of Yb_2Pt_2Pb crystallizing in the tetragonal U_2Pt_2Sn-type structure, a superstructure derived from the tetragonal Mo_2FeB_2-type structure common to most of the R_2T_2M (R=rare earths, T=transition metals, and M=Cd, In, Sn, and Pb). A comparison of the crystal structure with that of other compounds reveals that the radii of the T and M atoms together control the lattice parameters, and hence the overall valence of the Yb ions, which are trivalent in Yb_2Pt_2Pb. The crystal structure implies a layered magnetic structure, with the Yb ions contained in two different planes with identical symmetry but different Yb-Yb spacings. In both, the moments lie on contiguous isosceles triangles, which can be mapped onto the Shastry-Sutherland model. Strong magnetic anisotropy is found at low temperatures with $\chi_{[100]}/\chi_{[001]} \sim 30$, indicating that the magnetic moments of the Yb ions are confined to planes and likely lie along the [110] and $[1\bar{1}0]$ directions. The magnetic structures implied by the magnetization measurements feature planes of orthogonal Yb dimers that lead to spin liquid ground states in other Shastry-Sutherland lattice systems.

Long range antiferromagnetic order occurs at 2.07 K, which emerges from a paramagnetic state which magnetic susceptibility, electrical resistivity, and specific heat measurements find to have substantial short range order and frustration. These experimental findings suggest that Yb_2Pt_2Pb may be a rare example of a Shastry-Sutherland lattice system, although additional experimental work is required to demonstrate this definitively.

ACKNOWLEDGMENTS

The authors are grateful to C. Broholm and P. Schiffer for useful discussions and to C. Henderson for assistance with the electron-probe microanalysis, which was performed at the University of Michigan Electron Microbeam Analysis Laboratory (EMAL). Work at the University of Michigan and at Stony Brook University is supported by the National Science Foundation under Grant No. NSF-DMR-0405961.

[1] R. A. Gordon, Y. Ijiri, C. M. Spencer, and F. J. DiSalvo, J. Alloys Compd. **224**, 101 (1995).
[2] P. de V. du Plessis, A. M. Strydom, R. Troć, and L. Menon, J. Phys.: Condens. Matter **13**, 8375 (2001).
[3] D. Kaczorowski, P. Rogl, and K. Hiebl, Phys. Rev. B **54**, 9891 (1996).
[4] M. Giovannini, H. Michor, E. Bauer, G. Hilscher, P. Rogl, and R. Ferro, J. Alloys Compd. **280**, 26 (1998).
[5] A. Doğan, S. Rayprol, and R. Pöttgen, J. Phys.: Condens. Matter **19**, 26609 (2007).
[6] S. K. Dhar, R. Settai, Y. Ōnuki, A. Gavatanu, Y. Haga, P. Manfrinetti, and M. Pani, J. Magn. Magn. Mater. **308**, 143 (2007).
[7] E. Bauer, H. Hilscher, H. Michor, Ch. Paul, Y. Aoki, H. Sato, D. T. Adroja, J.-G. Park, P. Bonville, C. Godart, J. Sereni, M. Giovannini, and A. Saccone, J. Phys.: Condens. Matter **17**, S999 (2005).
[8] R. Hauser, H. Michor, E. Bauer, G. Hilscher, and D. Kaczorowski, Physica B (Amsterdam) **230-232**, 211 (1997).
[9] L. Havela, V. Sechovský, P. Svoboda, M. Diviš, H. Nakotte, K. Prokeš, F. R. de Boer, A. Purwanto, R. A. Robinson, A. Seret, J. M. Winand, J. Rebizant, J. C. Spirlet, M. Richter, and J. Eschrig, J. Appl. Phys. **76**, 6214 (1994).
[10] R. Pöttgen, Z. Naturforsch., B: Chem. Sci. **49**, 1525 (1994).
[11] R. Pöttgen, Z. Naturforsch., B: Chem. Sci. **49**, 1309 (1994).
[12] P. Gravereau, F. Mirambet, B. Chevalier, F. Weill, L. Fournès, D. Laffargue, F. Bourée, and J. Etourneau, J. Mater. Chem. **4**, 1893 (1994).
[13] L. C. J. Pereira, J. M. Winand, F. Wastin, J. Rebizant, and J. C. Spirlet, *24iémes Journées des Actinides* (Obergurgl, Austria, 1994), Abstract PB.9.
[14] F. Hulliger, J. Alloys Compd. **232**, 160 (1996).
[15] R. Pöttgen, P. E. Arpe, C. Felser, D. Kußmann, R. Müllmann, B. D. Mosel, B. Künnen, and G. Kotzyba, J. Solid State Chem. **145**, 668 (1999).
[16] B. S. Shastry and B. Sutherland, Physica B (Amsterdam) **108**, 1069 (1981).
[17] S. Miyahara and K. Ueda, Phys. Rev. Lett. **82**, 3701 (1999).
[18] H. Kageyama, K. Yoshimura, R. Stern, N. V. Mushnikov, K. Onizuka, M. Kato, K. Kosuge, C. P. Slichter, T. Goto, and Y. Ueda, Phys. Rev. Lett. **82**, 3168 (1999).
[19] H. Kageyama, K. Onizuka, T. Yamauchi, Y. Ueda, S. Hane, H. Mitamura, T. Goto, K. Yoshimura, and K. Kosuge, J. Phys. Soc. Jpn. **68**, 1821 (1999).
[20] J. Etourneau, J. P. Mercurio, A. Berrada, and P. Hagenmuller, J. Less-Common Met. **67**, 531 (1979).
[21] S. Michimura, A. Shigekawa, F. Iga, M. Sera, T. Takabatake, K. Ohoyama, and Y. Okabe, Physica B **378-380**, 596 (2006).
[22] S. Yoshii, T. Yamamoto, M. Hagiwara, A. Shigekawa, S. Michimura, F. Iga, T. Takabatake, and K. Kindo, J. Phys.: Conf. Ser. **51**, 59 (2006).
[23] F. Iga, A. Shigekawa, Y. Hasegawa, S. Michmura, T. Takabatake, S. Yoshii, T. Yamamoto, M. Hagiwara, and K. Kindo, J. Magn. Magn. Mater. **310**, e443 (2007).
[24] F. Hulliger, J. Alloys Compd. **217**, 164 (1995).
[25] G. Melnyk, H. C. Kandpal, L. D. Gulay, and W. Tremel, J. Alloys Compd. **370**, 217 (2004).
[26] R. Pöttgen, A. Fugmann, R. Hoffmann, U. Ch. Rodewald, and D. Niepmann, Z. Naturforsch., B: Chem. Sci. **55**, 155 (2000).
[27] N. Tsujii, H. Kitô, H. Kitazawa, and G. Kido, J. Alloys Compd. **322**, 74 (2001).
[28] M. Giovannini, E. Bauer, H. Michor, G. Hilscher, A. Galatanu, A. Saccone, and P. Rogl, Intermetallics **9**, 481 (2001).
[29] T. Muramatsu, T. Kanemasa, E. Bauer, M. Giovannin, T. Kagayama, and K. Shimizu, arXiv:0704.3307 (unpublished).
[30] I. R. Fisher, Z. Islam, and P. C. Canfield, J. Magn. Magn. Mater. **202**, 1 (1999).
[31] M. E. Fisher and J. S. Langer, Phys. Rev. Lett. **20**, 665 (1968); S. Alexander, J. S. Helman, and I. Balberg, Phys. Rev. B **13**, 304 (1976).
[32] M. Albrecht and F. Mila, Europhys. Lett. **34**, 145 (1996).
[33] C. H. Chung, J. B. Marston, and S. Sachdev, Phys. Rev. B **64**, 134407 (2001).
[34] K. Prokeš, P. Svoboda, A. Kolomiets, V. Sechovský, H. Nakotte, F. R. de Boer, J. M. Winand, J. Rebizant, and J. C. Spirlet, J. Magn. Magn. Mater. **202**, 451 (1999).
[35] J. A. Blanco, P. J. Brown, A. Stunault, K. Katsumata, F. Iga, and S. Michimura, Phys. Rev. B **73**, 212411 (2006).
[36] Z. Fisk, M. B. Maple, D. C. Johnston, and L. D. Woolf, Solid State Commun. **39**, 1189 (1981).
[37] A. Isacsson and O. F. Syljuåsen, Phys. Rev. E **74**, 026701 (2006).